Received: 23 November 2022 | Revised: 17 March 2023 | Accepted: 17 March 2023

DOI: 10.1002/nano.202200243

RESEARCH ARTICLE

nano select Open Access WILEY

Characterization and quantification of oxidative stress induced particle debris from polypropylene surgical mesh

Nicholas T. H. Farr[1,2] | **Cassandra Rauert**[3] | **Alexander J. Knight**[4] | **Alexander I. Tartakovskii**[4] | **Kevin V. Thomas**[3]

[1]Department of Materials Science and Engineering, University of Sheffield, Sheffield, UK

[2]Insigneo Institute for In Silico Medicine, The Pam Liversidge Building, Sheffield, UK

[3]Queensland Alliance for Environmental Health Sciences (QAEHS), The University of Queensland, Woolloongabba, Australia

[4]Department of Physics and Astronomy, University of Sheffield, Sheffield, UK

Correspondence
Nicholas T. H. Farr, Department of Materials Science and Engineering, Sir Robert Hadfield Building, Mappin Street, University of Sheffield, Sheffield S1 3JD, UK.
Email: n.t.farr@sheffield.ac.uk

Funding information
Engineering and Physical Sciences Research Council, Grant/Award Numbers: EP/V012126/1, EP/T517835/1; Medical Research Council (MRC); Minderoo Foundation

Abstract

Explanted polypropylene (PP) surgical mesh has frequently been reported to show surface alterations, such as cracks and flaking. However, to date the consequence of PP mesh degradation is not clearly understood, particularly its potential to influence the biological host response of surrounding tissues. Of particular concern is a possible host reaction to polypropylene particles released through degradation of surgical mesh in vivo. This concern is driven by previous studies which have postulated that an oxidative stress environment has the potential to etch away particles from the surface of a PP fibers. The release of such particles is of considerable significance as particles in the nano- to micro range have been shown to have the capacity to irritate cells and stimulate the immune system. The authors are not aware of any previous studies that have attempted to characterize, quantify or identify any particles released from PP mesh after exposure to an oxidative stress environment. Characterization of the PP mesh, post oxidative stress exposure, including identification of particles was achieved through application of a range of techniques: low voltage-scanning electron microscopy (LV-SEM), pyrolysis gas chromatography mass spectrometry (Pyr-GCMS), nano-Fourier transform infrared spectroscopy (nano-FTIR), scattering-type, scanning near-field optical microscopy (s-SNOM), atomic force microscopy (AFM), attenuated total reflectance-Fourier transform infrared spectroscopy (ATR-FTIR) and uniaxial tensile testing. The findings of this study indicate that oxidative stress alone is a major factor in the production of PP particle debris. PP debris identified within solution, using Pyr-GCMS, was shown to be in order of the micron scale.

KEYWORDS
debris, degradation, materials characterization, particles, pelvic organ prolapse, polypropylene mesh, stress urinary incontinence, transvaginal mesh

1 | INTRODUCTION

Since the 1950s abdominal wall hernias, including incisional and inguinal hernias have been routinely repaired using a polypropylene surgical mesh.[1] Based on the success of this technique, gynecologists in the 1970s applied PP meshes for pelvic organ prolapse (POP) and within 20 years PP meshes were also being used for the treatment of stress urinary incontinence (SUI).[2] The use of PP surgical mesh for transvaginal repair of POP was contemporary with SUI deployment. Surface alterations, such as cracks and flaking, materializing on explanted PP mesh have been frequently reported.[3,4] Synergistic effects of corrosive chemicals produced by inflammatory cells, such as reactive oxygen species (ROS),[5] together with mechanical stress applied to mesh threads in vivo is considered to result in degradation of PP mesh fibers.[6] PP interaction with immune cells is influenced as a consequence of this altered morphology.[7,8] Long-term safety concerns have been raised regarding PP mesh implants as a consequence of the findings of both patient outcomes and in vitro studies.[9,10]

To date, the effects of mesh degradation on the biological host response is not yet clear. A recent study from the authors of this paper has previously postulated a process whereby oxidative stress has the potential to etch away PP particles from the surface of a PP fiber.[10] The release of such particles is of great interest to researchers as particles in the nano- to micron range have been shown to have the capacity to irritate cells and stimulate the immune system.[7] These particles may contribute to tissue inflammation via surface enlargement and are considered as a viable explanation for the relatively strong foreign body reaction provoked by PP mesh. Although it is widely acknowledged that the existence of degraded polymeric particles and their potential influence on cellular tissues merits research effort,[11] no study to date has focused on confirming the existence of degraded PP particles from surgical mesh. The most notable evidence for in vivo PP particle production was the discovery of the presence of blue granules (thought to be from a surgical mesh fiber dye) observed within a histological section of an explanted Ethicon transvaginal mesh.[3] A recent study published by the authors applied secondary electron hyperspectral imaging and x-ray photoelectron spectroscopy to identify oxidation products on the surface of PP meshes after mechanical distention.[10] These results showed that by substituting dH_2O with H_2O_2, oxidation of the materials was notably increased. Additionally, Gel permeation chromatography revealed that mechanical distention with H_2O_2 treatment produced insoluble products, thought to be highly cross-linked regions of PP. It has therefore been proposed that PP particles have the potential to be "etched" away from the fiber surface due to oxidation through molecular chain scission. However, no study to date has confirmed the size of these particles or provided any strong evidence as to if and how they become detached from the PP fiber surface. Additionally, a mechanism explaining how such particles would be formed has not been established; is particle formation solely related to oxidative stress or is there also a relationship to mechanical wear? It is necessary therefore to consider the formation of PP debris particles and the mechanism of how they are released into the implantation environment as two interrelated issues.

To answer these questions, the role of oxidative stress in surface alterations needs to be evaluated separately from the role of mechanical stress input. This study is therefore focused on the characterization and quantification of oxidative stress induced particle debris from PP surgical mesh. With an additional aim to observe whether surface modification resulting from oxidative stress degradation has any effect on bulk chemistry or mechanical properties of the mesh. To achieve these aims characterization of the PP mesh post oxidative stress exposure, including identification of particles, was achieved through the application of a range of techniques: low voltage-scanning electron microscopy (LV-SEM), pyrolysis gas chromatography mass spectrometry (Pyr-GCMS), atomic force microscopy (AFM), nano-Fourier transform infrared spectrscopy (nano-FTIR), Fourier transform infrared spectroscopy (ATR-FTIR), and uniaxial tensile testing.

2 | MATERIALS AND METHODS

A workflow of the experimental set up is presented in Figure 1.

2.1 | Materials

A commercially available material, Prolene® Mesh (Ethicon), fabricated from PP was chosen for this study. Proplene® Mesh is routinely selected for clinical repair of abdominal hernias. Three sample strips of the material were cut using sterilized scissors within a cell culture cabinet along the longitudinal direction of the surgical mesh. Samples 1 and 2 had dimensions of 50 × 30 mm. Sample 3 had a dimension of 20 × 20 mm.

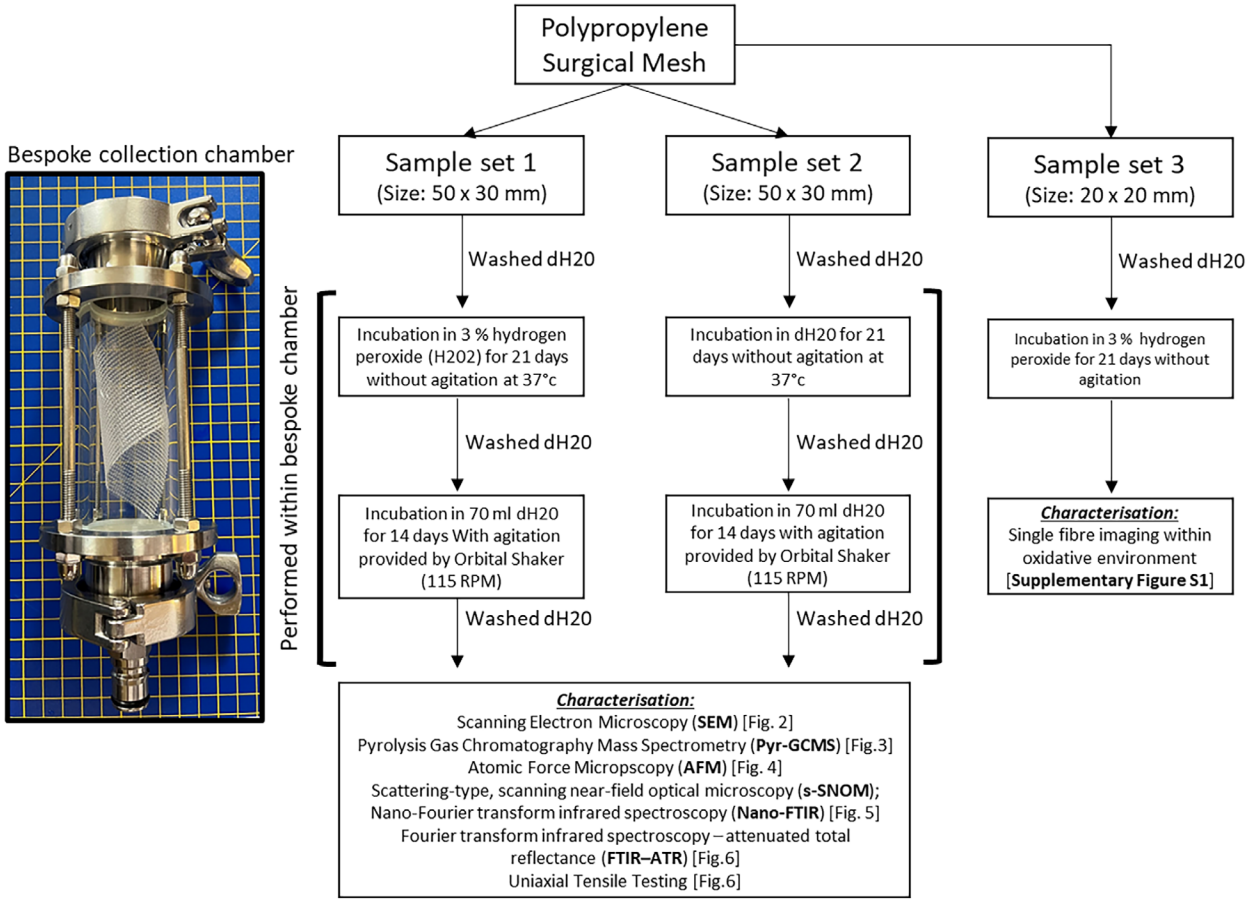

FIGURE 1 Workflow of the experimental set up.

2.2 | Use of a bespoke stainless steel collection chamber

As the study was focused on identifying PP surface particles it was imperative to eliminate the risk of other polymer sources contaminating the study samples. In order to reduce the likelihood of contamination of the polymer mesh by way of the collection vessel a collection chamber was fabricated (Figure 1). With a max volume of 250 mL, the collection chamber was fabricated from chemical grade glassware and stainless steel (following ISO standard[12]). The customization of an in-line sight glass with clamp ends comprising of a 304 stainless steel body was selected due to its ability to withstand H_2O_2 corrosion. The inspection chamber was used in all stages of particle isolation, including accelerated oxidative stress degradation and dH_2O orbital shaking.

2.3 | Oxidative stress induced by an accelerated degradation test

As described in Figure 1, Sample 1 was subject to an accelerated degradation test. The procedures adopted for the study were conducted in accordance with the recommendations of *ISO 10993-13, Biological Evaluation of Medical Devices—Part 13*: Identification and Quantification of Degradation Products from Polymeric Medical Devices.[12] Sample 1 (8 g of mesh) was placed in the stainless steel collection chamber with an appropriate volume (80 mL) (test article solution ratio of 1 g :10 mL) of 3% hydrogen peroxide (H_2O_2) (hydrogen peroxide solution, contains inhibitor, 30 wt% in H_2O, ACS reagent, Sigma-Aldrich. Sample 1 was then incubated at 37°C for 21 days without agitation. Both temperature and the time duration selected came as a result of reference to ISO standards and previous studies.[10,12] After the accelerated degradation treatment, sample 1 was then washed with dH_2O and placed into a cleaned collection container. This chamber was then loaded onto an orbital shaker for 14 days at 115 RPM to allow for gentle agitation. Identical treatment conditions were applied to the control sample 2, however, instead of an incubation period in H_2O_2, sample 2 was incubated in dH_2O. At the end of the 14 days' treatment the PP meshes were removed from their collection chambers and the dH_2O incubation solution was stored in glass vials prior to Pyr-GCMS analysis.

2.4 | Low voltage (LV)-SEM imaging

FEI Helios Nanolab G3 (FEI Company, US) and Helios G4 DualBeam (ThermoFisher Scientific, US) microscopes were employed for surface morphology observations of PP mesh samples 1 and 2. In contrast to common SEM analysis practice, the samples were not pre-treated with a conductive coating by deposition. An accelerating voltage of 1–2 keV at typical chamber vacuum pressures in the range of 10^{-6} mbar and a working distance of 4–8 mm was chosen to avoid sample damage through surface charging. An Everhart-Thornley detector (ETD) was selected for high-magnification SE images.

2.5 | Atomic force microscopy (AFM)

AFM microscopy was performed in tapping mode with SCANASYST-AIR probes under ambient conditions on a Bruker Dimension Icon AFM. PP mesh samples were placed on a cover glass and then attached to a magnetic AFM support. Different areas of the samples were then analyzed and characterized to produce peak force images. Peak force error images are the characteristic of PeakForce Tapping AFM mode, where the maximum value of the tip-surface interaction force is used as a constant setpoint for each pixel of the area scanned.[13] Data analysis was then performed using the Bruckers NanoScope Analysis software (Version 2.0).

2.6 | Nano-Fourier transform infrared spectroscopy (nano-FTIR); scattering-type, scanning near-field optical microscopy (s-SNOM); and associated atomic force microscopy (AFM)

Nano-FTIR, s-SNOM, and AFM data were collected using a neaSCOPE from attocube systems AG/Neaspec, all under ambient conditions.

Nano-FTIR spectra: Light from a broadband illumination source (FemtoFiber dichro midIR from TOPTICA Photonics, roughly across the wavenumbers 700–1850 cm^{-1}) was sent into a Michaelson interferometer, with an AFM and sample in one interferometer arm and a reference mirror in the other. A conductive AFM cantilever (Pt/Ir coated ARROW-EFM tip from NanoWorld) was brought into tapping mode operation upon the sample (tapping frequency 83.2 kHz, tapping amplitude 81–82 nm), and the cantilever tip and sample were illuminated with the broadband source. Under illumination, the conductive cantilever tip acts as an optical antenna and a near field is generated at the tip apex (radius around 25 nm). The near field interacts with the sample surface and forms a scattering center that scatters further incoming photons. The scattered photons were collected at a detector and interfered with photons returning from the reference mirror. A lock-in detector was used to demodulate the detected signal at the second harmonic of the AFM tapping frequency to reduce the influence of background-scattered light. By moving the reference mirror along the beam path by a given distance (400 μm at a speed of 7.8 μm s^{-1}) an interferogram was recorded, which was then converted into optical amplitude and phase spectra via a Fourier transform. In order to account for the instrument response (such as the output of the spectrum of the illumination source), the recorded data was then normalized to a measurement of a spectrally flat test sample (silicon material, made immediately after the sample measurements). Four repeat scans were done for each measurement spot and averaged. In order to account for thermal drift in the system between the sample measurement and reference measurement (especially in the interferometer arms), a linear gradient and a constant offset were subtracted from the optical phase spectra.

s-SNOM: Light from a single-wavelength source (MIRcat-QT from Daylight Solutions) was used in the same setup as described for the nano-FTIR measurements above. A movable mirror in the reference arm was oscillated in order to induce side-band frequency mixing in the raw optical signal power spectrum, and the optical amplitude and phase data were extracted at the third harmonic of the AFM tapping frequency (83.5 kHz, at an amplitude of 73–76 nm). The optical amplitude data were normalized to the maximum recorded value, and the optical phase data were offset by the value recorded from a silicon reference measurement made immediately before the presented s-SNOM scan.AFM data: AFM topology data were recorded using the same neaSCOPE from attocube systems AG/Neaspec as used for the nano-FTIR and s-SNOM measurements. Conductive AFM cantilevers (Pt/Ir coated ARROW-EFM tip from NanoWorld) were used, and the corresponding tapping amplitudes are listed above.

2.7 | Attenuated total reflectance-Fourier transform infrared spectroscopy (ATR-FTIR)

Infrared spectra were obtained for both samples 1 and 2 using a NICOLET 380 FTIR spectrometer (ThermoFisher Scientific, US). Purged with dry air before spectra collection in the range from 500 to 4,000 cm^{-1} averaging 32 scans and a resolution of 4 cm^{-1}. The samples were analyzed in their solid-state form using an attenuated total reflection

(ATR) accessory with a Golden Gate® diamond crystal (Specac, UK).

2.8 | Uniaxial tensile testing

Uniaxial ramp testing was performed for samples 1 and 2 after accelerated degradation and dynamic distention conditions. A tensiometer (MultiTest-dV, Mecmesin) was used. Test pieces from samples 1 and 2 ($n = 4$, for each material) were clamped between two grips of the tensiometer with a testing length of 10 mm. A load cell of 250 N was used. The sample meshes test pieces were loaded in the longitudinal direction, in the direction of use as indicated by the manufacturer. A tensile test was then applied at a rate of 0.1 mm s^{-1}. All experiments were performed under constant laboratory conditions (23°C, British air humidity 80%).

2.9 | Pyrolysis gas chromatography mass spectrometry

Polypropylene particles present in the incubation solutions were quantified using Pyr-GCMS. First, the solutions were filtered onto a 0.3 μm glass fiber filter (GF-75 21 MM, Labtek Pty. Ltd., Brendale, Australia). The filter papers were individually rolled and inserted into an 80 μL pyrolysis cup (Eco-Cup LF, Frontier Laboratories, Japan). The sample cups were spiked with 40 μg of deuterated polystyrene (d_5-PS, Polymer Source Inc., Dorval, Canada) as an internal standard before analysis. Samples were analyzed with a multi-shot micro-furnace pyrolyzer (EGA/PY-3030D) coupled with a GC2030 GCMS (Shimadzu Corporation, Japan), using a double shot method and data were collected in full scan mode over a mass range of 40 to 600 m z^{-1}, following previously reported methodologies.[14] The polypropylene pyrolysis product 2,4-dimethyl-1-heptene was monitored (m/z 126, 83, 70) to quantify the mass of polypropylene in each sample.

2.10 | Statistical analysis

Statistical analysis and graph production was performed using the GraphPad Prism version 9 software (GraphPad Software, Inc.; La Jolla, USA). Data are reported as mean ± standard deviation. The significance level was defined as $p < 0.05$. For nonparametric analysis, the Mann–Whitney test was used for data that was not normally distributed.

3 | RESULTS AND DISCUSSION

3.1 | Assessment of surface morphology

In most applications where plastics are susceptible to degradation this is first initiated at the polymer surface, which is exposed and available for chemical (H_2O_2 in this study) or cellular/enzymatic attack (in vivo), therefore surface analysis is integral for the study of polymer degradation.[15] In order to assess the surface morphology of PP meshes, a series of SEM images were obtained and presented in Figure 2 (methodology recommended by ISO 10993-18). SEM imaging was performed on uncoated samples 1 and 2 to which no addition conductive coating was applied. This approach was selected to ensure that the images were direct visualizations of the surface morphology of the meshes.

From the images presented in Figure 2, it is apparent that surface degradation is discernible on both PP sample meshes. For both samples SEM images presented showed surface markings on the fiber strands, these markings are not unexpected and are a consequence of the fabrication process for the knitted fiber mesh. However, surface marking is less apparent in SEM images obtained from PP + dH_2O (Figure 2A,B), than that of PP + H_2O_2 (Figure 2C–E). Figure 2A–D images were all obtained using the same magnification and therefore are directly comparable in length scales. Figure 2C images distinctly shows the formation of PP surface particles which can be seen predominantly within the micron size (5–10 μm) length scale. Observable PP particles are localized around areas of what appears to be oxidative induced surface degradation of the mesh fibers. This is commonly observed in vivo as studies have shown that the secretion of ROS from cells can lead to surface oxidation and embrittlement.[16] The SEM images presented are consistent with previously published images,[10] both in terms of the range of particle size and surface morphology features, post oxidative stress treatment. Figure 2E shows a lower magnification SEM image of PP + H_2O_2 mesh samples. In this image, it can be observed how extensive the formation of particles is and also the multi-length scale of the particles (highlighted with a red circle) in comparison to the underlying PP fiber. It should be noted that these particles have not formed specifically within areas of high-stress load (e.g., Knot sites), but instead have formed universally across the fibers. This finding provides evidence to support the proposition that oxidation stress can independently promote the formation of PP debris particles without the contribution of mechanical abrasion/wear, a mechanism which is known to be a common process of producing particle debris.[17,18] Aside from

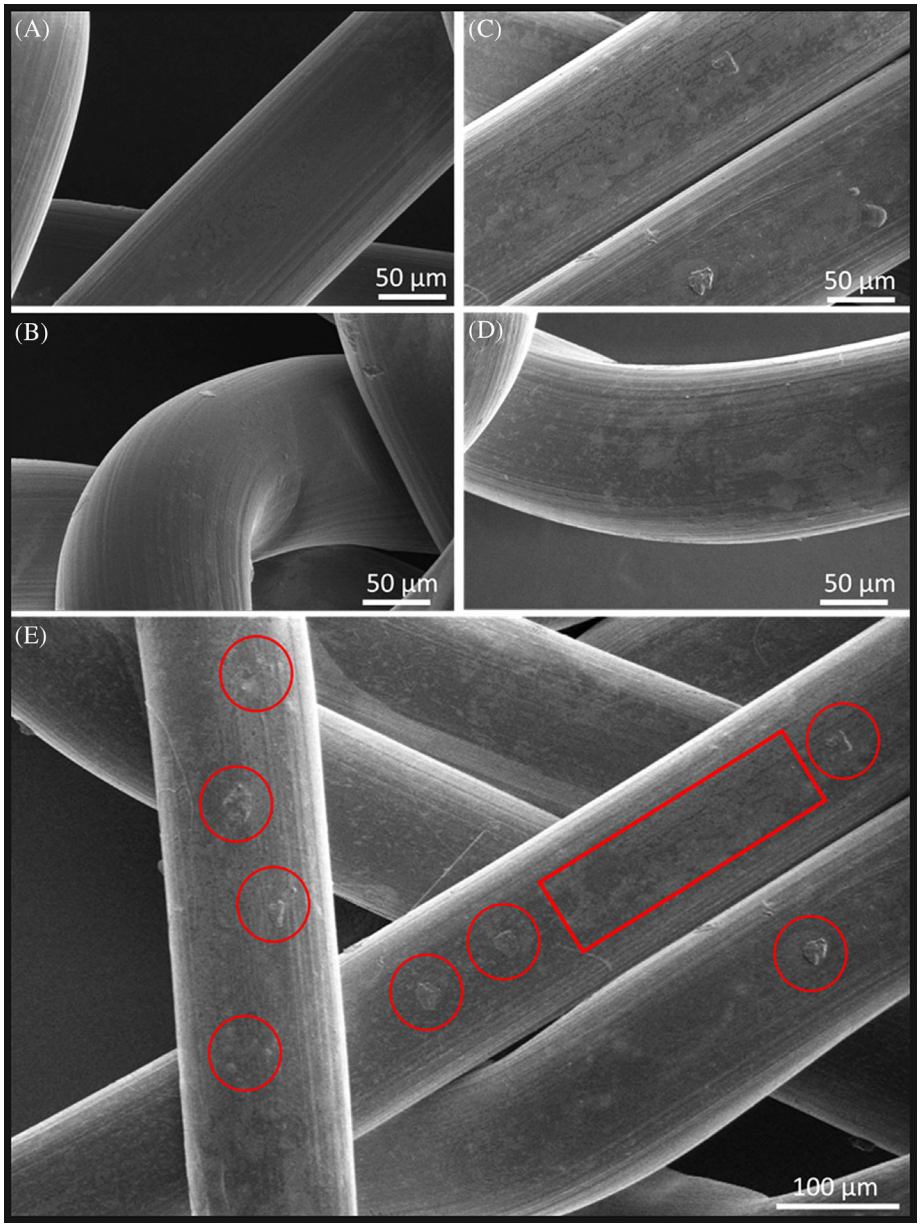

FIGURE 2 Collection of SEM images of PP the after dH_2O incubation (A, B) and H_2O_2 accelerated degradation (C–E).

particle formation Figure 2E also shows surface degradation (highlighted by rectangular box) in various locations on the mesh surface. Comparable to the locations of the observed PP particles, surface degradation can be seen to be not localized within high-stress regions of the mesh instead it is also observed as a consistent feature in all areas of the PP fiber.

3.2 | Pyrolysis gas chromatography mass spectrometry and atomic force microscopy

Polypropylene was detected in all three incubation solutions (Figure 3A), however, concentrations were more than 300 x higher in the PP + H_2O_2 mesh sample (32 µg/sample) than in the PP + dH_2O sample or the control (blank) sample (0.1 and 0.02 µg/sample, respectively). It is noted that only particles >300 nm were collected on the filter and quantified, and smaller particles may have also been present in the samples.

The identification of micron sized particles raises many clinically related concerns. Key questions in respect to the effect that such micro-plastic particles have on the human health are yet to be fully quantified. However, interest in studying micro-plastics is growing in step with concerns of increasing plastic pollution leading to more human exposure to micro-plastics.[19–21] Figure 3B presents previously published data which investigated the cellular responses to

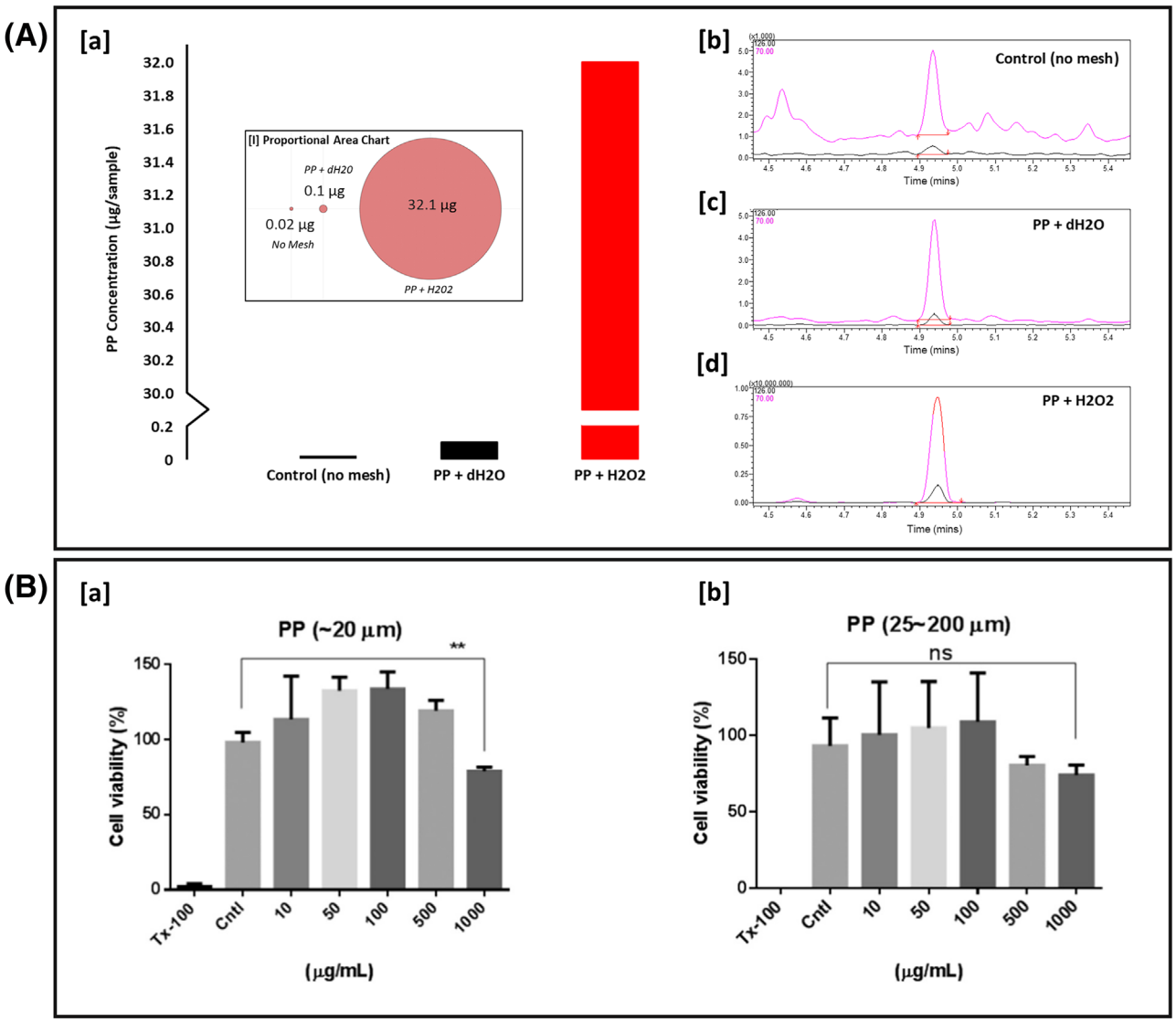

FIGURE 3 A, (a) Bar chart presenting results obtained from pyrolysis gas chromatography mass spectrometry (Pyr-GCMS) of incubation solutions from Control (no mesh), PP + dH_2O and PP + H_2O_2. Graphs (b–d) present Pyrograms of PP pyrolysis marker (2,4-dimethyl-1-heptane) in (b) Control, (c) PP + dH_2O, and (d) PP + H_2O_2. B, Reproduced and rescaled from ref.[7] under the Creative Commons Attribution International License (CC BY) http://creativecommons.org/licenses/by/4.0/ with permission from Elsevier. Cytotoxic effects of PP particles on Human dermal fibroblasts (HDFs). (a) Viability test for cells treated with ~20 µm PP particles (at different concentrations) in DMSO on HDF cells. (b) Viability test for cells treated with 25–200 µm PP particles (at different concentrations) in DMSO on HDF cells.

PP particles of approximately, ~20 µm and 25–200 µm.[7] This study found that size, rather than concentration, was the most important parameter governing the cytotoxic effects (Figure 3B). It was hypothesized that direct contact of PP particles with cells may have the potential to cause health problems by inducing the production of cytokines from immune cells.[7] Recent studies have demonstrated the toxicity of micro-plastics in vitro to lung, liver, and brain cells,[22] with in vivo studies showing that even low toxicity particle materials can stimulate pro-inflammatory activity as a consequence of their relatively large surface area to mass ratio.[23]

It has been widely reported that a hostile inflammatory environment can lead to surface alterations in polymer derived—biomaterials.[24,25] It was expected that PP degradation, as commonly observed in many plastics, would first occur at the polymer surface. Previous PP focused studies have shown that uncoated PP mesh can provoke a dominant M1 macrophage response at the PP mesh fiber surface.[26] The specific macrophage activation will determine the healing process. An M1 macrophage phenotype has been associated with a chronic immune response and material rejection, leading to an increased formation of fibrotic tissue.[27] It is considered feasible that PP particles

of micron scale size released into the in vivo mesh environment may instigate the inflammation of nearby cells which in turn release additional oxidizing agents. This PP degradation/inflammation cycle would then have the potential to drive a positive feedback loop significantly increasing the expected immune response. Recent studies focused on the toxicology of PP material have indeed shown that PP alone has the potential to trigger an increase in cell inflammation which in turn leads to an increase in PP fiber oxidation products.[7] The clinical effect of PP particles in vivo is likely to be dependent on many factors, including: dose, surface chemistry, hydrophobicity, and ultimately particle size. The filtration method used in this study shows the abundance of micron scale particles released through PP degradation, however, studies have also shown that nano-sized polymer particles can also have a deleterious effect on human health associated with their ability to pass through cell membranes and epithelium layers.[28] The reduction in PP particle size through continuously repeated cycles of oxidative stress, opens the possibility of induced novel particle characteristics, including influences to their potential toxicity.[19]

To investigate the presence of nano-particles on the surface of the PP mesh sample fibers AFM was performed. Figure 4A,B shows AFM images of PP + dH_2O and PP + H_2O_2 retrospectively. From the 2D peak force images presented an increase in the variation of the surface roughness and particle formation is clearly observable in PP + H_2O_2 when compared to that of PP + dH_2O. The surface topography of PP + dH_2O contains longitudinal surface markings consistent with the direction of stress applied during mesh fabrication. PP + H_2O_2 contains similar longitudinal markings, however circular features and deep surface cracks/craves are also apparent at varying length scale. It is well established that one of the first visual effects of polymer degradation is the creation of surface crazes[29] which are a precursor to a structural crack. Polymer crazing is a phenomenon observed during a creep period when load is applied.[30] In this instance, it is considered that nanoscale crazing first occurs during the mesh fabrication process (markings visible in Figure 4A). Mesh implantation within an oxidative stress environment, in this study H_2O_2, further promotes an increase in surface crazing through exposure to oxidative degradation processes. The formation of crazes not only acts as a precursor to larger structural surface cracking, which are expected to affect the mesh material's mechanical properties,[31] but also can act as a pathway for bulk polymer oxidation. Eventually, surface cracking propagates and exposes greater surface areas thereby making more material available for further degradation. This process ultimately leads to embrittlement and fragmentation of the polymer.[29] Nanoscale circular features are identifiable across the PP fiber surface in addition to visible crazes. These surface features range in size from the nanoscale, to the micron scale at 0.1–1 μm sizes. In contrast to the formation of crazes there is no obvious trend discernible in the formation of these surface features, with no localized structural precursor visible. It is therefore considered that unlike the formation of crazes these surface features cannot be directly related to the application of mechanical stress during mesh fabrication.

Figure 4C displays a three-dimensional AFM topography image of a region of PP + H_2O_2. Within the 5 × 5 μm field of view it is notable that particles are present with variating peak heights. The majority of particles peaks found within this region are of a height of 100–130 nm range with a particle width of around 50 nm–2 μm. It is therefore considered that structures such as these, sized within the micron and nano scale, have the potential to become dislodged from the PP fiber surface and if at the correct length scale, identified by the filtration system. The possibility of nano plastics within the body has long raised concerns,[32] with effects of oxidative stress, cell damage and tissue inflammation.[33] Nano plastics have shown the capacity to enter cells irreversibly[34] and through endocytic pathways[35] and lipid membranes.[36] With the additional concern that nanoscale plastics have the capacity to cross membranes including the blood-brain barrier and the human placenta[37,38] From the AFM data presented it is expected that nanoscale particles also are present and have equal potential to also be released, particles in the nanoscale size range would evade the filter detection applied in this study. Aside from the formation of particles, it is observable from the 3D tomography images the extent of PP + H_2O_2 surface roughness caused by topography inconsistencies. An increase of the surface roughness of the PP material would also consequently increase the surface area of the material, exposing a greater surface area to the effects of oxidative degradation.

To identify any surface alterations within the chemical structure of PP + H_2O_2, nano-FTIR was collected from two regions on the PP + H_2O_2 surface (Figure 5A), one on and one off an identified PP particle feature (Figure 5B). Nano-FTIR phase data for both regions showed the appearance of previously published spectral PP peaks.[5,39,46–47] Of interest: (C-C (808 cm^{-1}), C-H (1166 cm^{-1}), and C = O stretch (1750–1500 cm^{-1}). Overall, both regions exhibit very similar nano-FTIR spectra, with slight variations in the positions and amplitudes of spectral peaks attributed principally to variations in the surface chemistry of the PP particles (notably at 1166 cm^{-1}, see below), although experimental variation due to water absorption and weak spectral power (at the ends of the wavenumber range) is noted. Figure S2 presents additional nano-FTIR spectra from points in Figure 5B, illustrating the low spot-to-spot

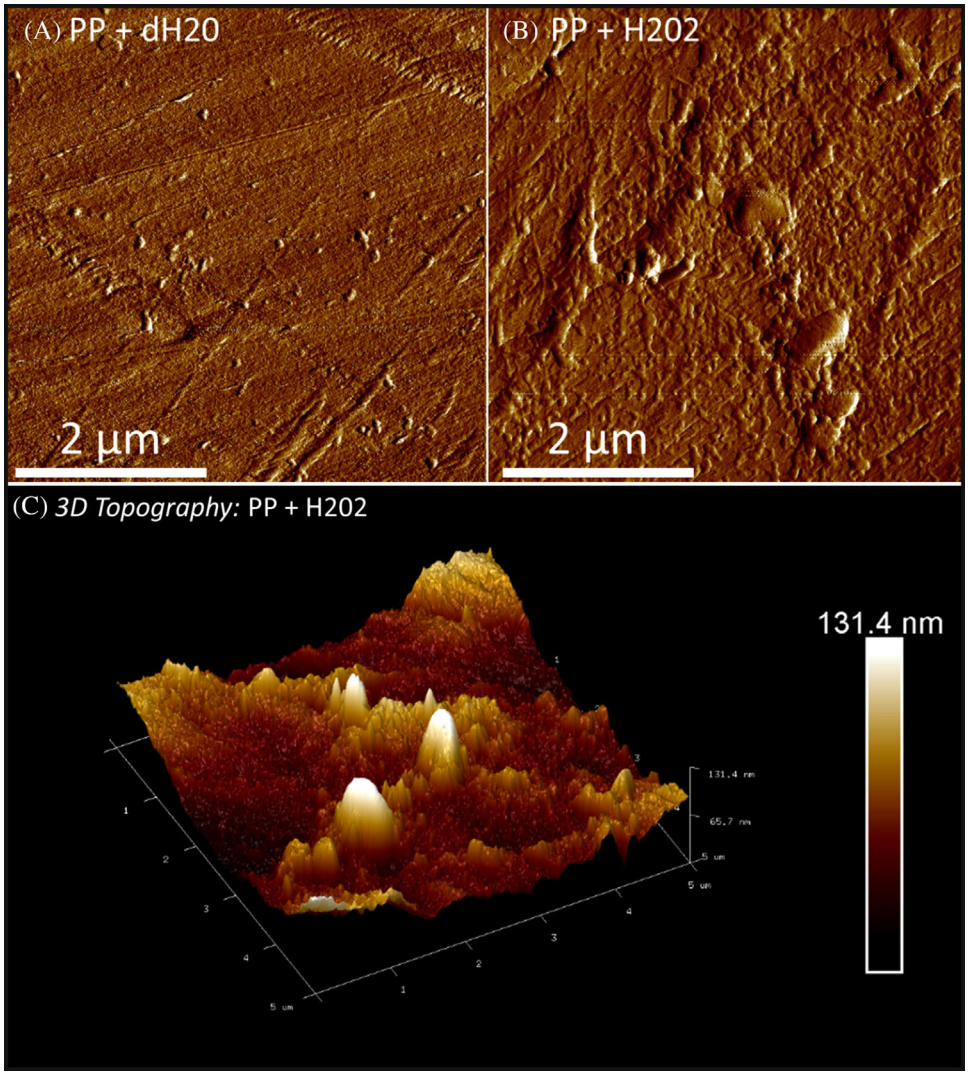

FIGURE 4 Atomic force microscopy (AFM) images taken using PeakForce Tapping mode. A, Presents an AFM peak error image of PP incubated in dH_2O and (B) after H_2O_2 accelerated degradation. C, 3D tomography map of PP after H_2O_2 accelerated degradation.

variation across the mesh and particles, and confirming that the experimental error is minimal. In vitro studies have established that the surface chemical composition of biomaterials have the ability to modify cell adhesion and the secretion of fibrogenic factors.[42–45] For PP specifically, studies have shown variating PP surface functionalization strongly influences fibrotic tissue reactions in vivo with an effect on tissue compatibility.[46]

As nano-FTIR is only capable of detecting surface properties across isolated spots, it can be challenging to understand the overall variation in surface chemistry from this type of data alone. In order to investigate further the slight spatial variations in surface chemistry highlighted by the nano-FTIR spectra in Figure 5A, scattering-type, scanning near-field optical microscopy (s-SNOM) was performed across a PP particle. An illumination wavenumber of 1166 cm^{-1} was selected (illustrated by the dotted line in Figure 5A), corresponding to a C-H absorption feature/CHx.[41] Figure 5C–E shows the AFM topography, s-SNOM amplitude data, and s-SNOM phase data, respectively, recorded from the PP particle. A large variation in both the optical amplitude and phase was observed across differing regions of the PP particle, indicating a large variation in surface chemistry related to the C-H bond, which could not be distinguished from the topography (Figure 5C). s-SNOM optical phase data are commonly associated with absorption, thus indicating that different regions of the PP particle were absorbing at much increased and much decreased levels as compared to the PP mesh surface, linked to the density of C-H bonds in these regions. Significant variations in the surface chemistry were not only present between PP mesh and PP particle, but also across the individual particles themselves indicating a much higher degree of chemical variation. One possible explanation for the results shown in Figure 5 is that the PP particles have experienced a loss of C-C

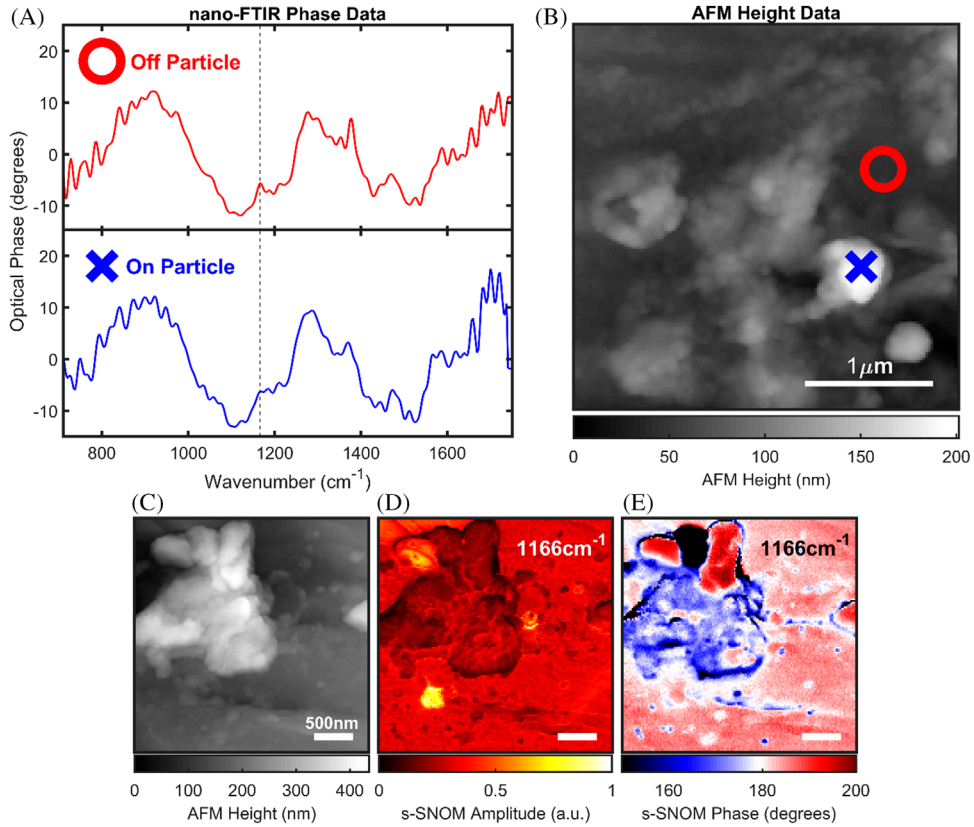

FIGURE 5 Nano-FTIR spectra (A), and AFM topological data (B) taken from the surface of a PP + H_2O_2 mesh. The top and bottom spectra in (A) were taken off and on a particle feature on the mesh surface, respectively, indicated by the corresponding circle and cross marks in (B). AFM topography (C), s-SNOM amplitude data (D), and s-SNOM phase data (E) were taken from a different PP particle using illumination at 1166 cm^{-1}. The optical amplitude data in (D) were normalized to the maximum-recorded value, and the optical phase data in (E) were offset by the optical phase of silicon according to a reference measurement made immediately before the scan of the PP particle. Data were collected with a neaSCOPE from attocube systems AG/Neaspec, with the nano-FTIR data in (A) demodulated at the second harmonic of the AFM tapping frequency, and the s-SNOM data in (D), (E) demodulated at the third harmonic of the AFM tapping frequency, to reduce the influence of background-scattered light.

coupling, resulting in greater absorption from side-group mode r(CH_3), which previous studies have linked with a decrease in the degree of PP crystallinity.[40,47–48] As greater C-H bonding has been assigned to shorter chains in helical conformation,[47,49] this result could therefore indicate the resulting shed PP particles experience variations in crystallinity. Previous studies have proposed a mechanism by which molecular chain scission would favor the less crystalline regions, resulting in the formation of crystalline surface particles.[40]

To understand if the variations in surface chemistry observed on the nano-scale in Figure 5 had any effect on the bulk chemistry or mechanical properties of the PP mesh samples, both Fourier transform infrared spectroscopy (ATR-FTIR) and uniaxial tensile testing was performed and presented in Figure 6. ATR-FTIR is a recommended technique for determining the chemical structure of synthetic polymers used in medical devices in accordance with the guidelines of the ISO 10993-18:2020 standard. Results obtained from both techniques showed no significant difference in both the bulk chemistry or bulk mechanical properties of the PP fibers in response to oxidative stress. The data presented by ATR-FTIR analysis did not identify functional groups related to bulk PP oxidation. This result was expected as early-stage degradation has been previously been reported to be confined to surface structures.[10] However, it should be noted that PP surgical mesh used successfully for POP and SUI procedures would be expected to withstand both the oxidative and mechanical stresses of lifelong implantation without bulk degradation.

In respect to uniaxial testing, a non-significant increase in Young Modulus was obtained for PP + H_2O_2 compared to that of PP + dH_2O, however, this result is not unexpected as previous studies have obtained similar results from PP meshes when subjected to H_2O_2.[10] Nonetheless, these results have value as they act as a test standard for the use of the orbital shakers and their resulting mechanical

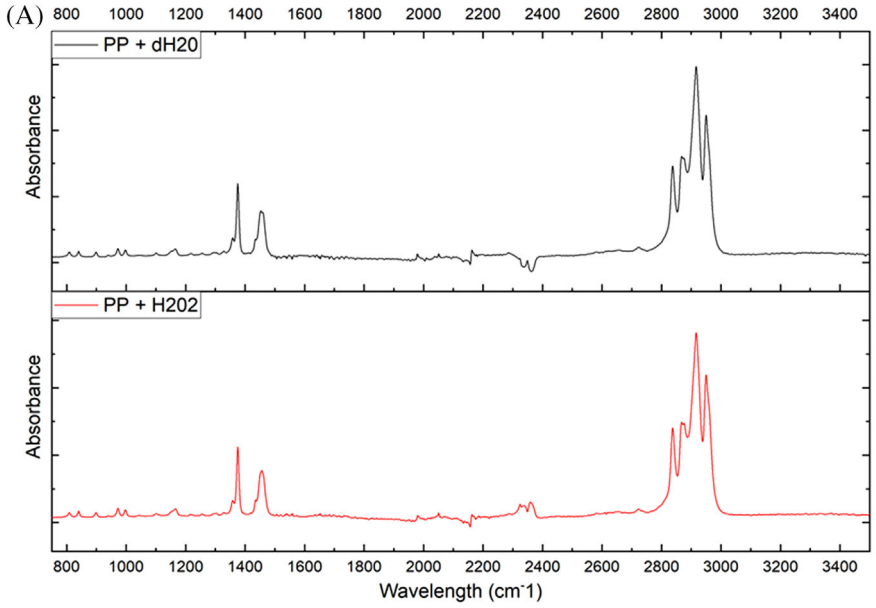

(B)

	PP + H202		PP + dH20	
	Max Stress (MPa)	Young's Modulus (MPa)	Max Stress (MPa)	Young's Modulus (MPa)
Mean	13.79	41.71	14.31	34.18
SD	1.58	6.27	0.832	1.15
Max	15.80	45.79	14.95	35.45
Min	12.38	32.45	13.16	32.91

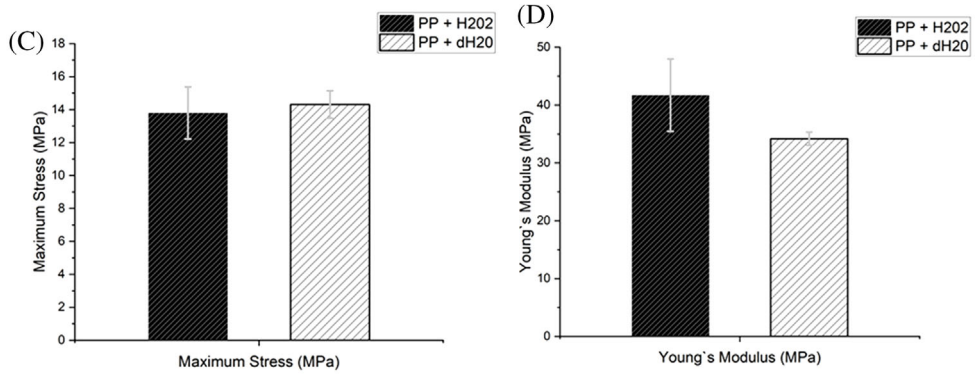

FIGURE 6 A, ATR-FTIR spectra collected from control (PP + dH_2O), and test (PP + H_2O_2) surgical meshes. B-C, A table (B) and (C) accompanying graphs showing Young's modulus and Max Stress of PP after dH_2O incubation and H_2O_2 accelerated degradation.

forces applied onto the mesh. The experimental set up of this study was chosen to isolate the contribution of oxidative stress on the production of PP degradation particles. It has been previously shown that mechanical distention can both effect PP surface morphology and also significantly affect the mechanical properties of PP fibers. With no significant difference found within the mechanical properties of PP after exposure to oxidative stress it can be confidently assumed that the mechanical stress applied by the orbital shaker to the PP mesh samples was minimal and had a limited effect in the production of PP particles. It is therefore postulated that the orbital shaker contributed to the removal of loosely attached PP surface fragments but did not affect the overall mechanical properties of the PP mesh samples. Within the clinical deployment environments of surgical mesh, any oxidative stress arising will be combined with the effect of host mechanical forces which are inevitably applied to the material in vivo. It is expected that these mechanical forces not only contribute to the physical removal of loosely attached particles, replicated in this study by use of an orbital shaker, but may also play a role in producing particles (via mechanical wear) directly. For future studies, it is necessary therefore to consider the formation of PP debris particles and the mechanism of how

they are released into the implantation environment as two interrelated issues.

4 | CONCLUSIONS

To the authors' knowledge, this is the first study to quantify oxidative stress induced debris from PP surgical mesh. The findings of the data presented indicate that oxidative stress alone is a major factor in the production of PP particle debris. PP debris identified within solution, using Pyr-GCMS, was shown to be in order of the micron scale. However, SEM and AFM surface imaging overcame filtration limitations and identified nanoscale particles which have the potential to also become cleaved from the fiber surface. Nano-FTIR and s-SNOM data presented shows that PP particles have a different—and highly diverse—surface chemistry compared to that of the regular oxidized surface. With previous studies having already raised concerns regarding the effect of nano-micron sized particles effect on human health, these findings emphasize the need for future studies to gain a deeper understanding of how macrophages and fibroblasts involved in the immune response, respond to this oxidative debris. Future studies should therefore consider these oxidative stress findings together with the application of mechanical distention through extending the test model to form a higher fidelity representation of the in vivo environment. Particular attention should be given to mechanically induced changes to surface morphology and the mechanism of particle shedding. Lastly, the effect of oxidative stress is not expected to be limited to PP, consideration should also be given to including a wider range of test materials encompassing all those used within pelvic floor reconstruction.

ACKNOWLEDGMENTS

Nicholas T.H. Farr would like to thank U.K funding bodies: Engineering and Physical Sciences Research Council (EPSRC) for funding (grant: EP/V012126/1 and EP/T517835/1) and the Medical Research Council (MRC) for funding provided through the confidence in concept scheme. Cassandra Rauert's salary is from the Minderoo Foundation, an independent not for profit philanthropic organisation. The Queensland Alliance for Environmental Health Sciences, The University of Queensland, gratefully acknowledges the financial support of Queensland Health. Nicholas T.H. Farr acknowledges the Sorby Centre for Electron Microscopy at the University of Sheffield for allowing electron microscopy and analysis to be performed. Alexander J. Knight and Alexander I. Tartakovskii acknowledge support by EPSRC grant EP/V007696/1.

CONFLICT OF INTEREST STATEMENT

The authors declare that there is no conflict of interest directly related to this article. This paper is an independent study. Neither Minderoo Foundation, nor its benefactors, had any influence over the conduct, the findings, or the recommendations of this paper.

DATA AVAILABILITY STATEMENT

The data that support the findings of this study are available from the corresponding author upon reasonable request.

REFERENCES

1. F. C. Usher, J. Ochsner, L. L. Tuttle, *Am. Surg.* **1958**, *24*, 969.
2. U. Ulmsten, L. Henriksson, P. Johnson, G. Varhos, *Int. Urogynecol. J.* **1996**, *7*, 81.
3. A. Imel, T. Malmgren, M. Dadmun, S. Gido, J. Mays, *Biomaterials* **2015**, *73*, 131.
4. V. V. Iakovlev, S. A. Guelcher, R. Bendavid, *J. Biomed. Mater. Res Part B: Applied Biomaterials* **2017**, *105*, 237.
5. H. J. Oswald, E. Turi, *Polym. Eng. Sci.* **1965**, *5*, 152.
6. D. Taylor, *J. Mech. Behav. Biomed. Mater.* **2018**, *88*, 370.
7. J. Hwang, D. Choi, S. Han, J. Choi, J. Hong, *Sci. Total Environ.* **2019**, *684*, 657.
8. D. L. Harrison, Y. Fang, J. Huang, *Front. Phys. 7*, 45, **2019**.
9. P. Dällenbach, *IJWH 331*, **2015**.
10. N. T. H. Farr, S. Roman, J. Schäfer, A. Quade, D. Lester, V. Hearnden, S. MacNeil, C. Rodenburg, *RSC Adv*. **2021**, *11*, 34710.
11. M. Thompson, S. Guelcher, R. Bendavid, V. Lakovlev, D. R Ostergard, *Int. Urogynecol. J.* **2017**, *28*, 333.
12. ISO 10993-13, Biological Evaluation of Medical Devices—Part 13: Identification and Quantification of Degradation Products from Polymeric Medical Devices.
13. G. Fakhrullina, F. Akhatova, M. Kibardina, D. Fokin, R. Fakhrullin, *Nanomedicine: NBM* **2017**, *13*, 483.
14. E. D. Okoffo, F. Ribeiro, J. W. O'Brien, S. O'Brien, B. J. Tscharke, M. Gallen, S. Samanipour, J. F. Mueller, K. V. Thomas, *Sci. Total Environ.* **2020**, *715*, 136924.
15. B. Gewert, M. M Plassmann, Leod Mac, *Environ. Sci.: Processes Impacts*, **2015**, *17*, 1513.
16. J. Kurtz, B. Rael, J. Lerma, C. Wright, T. Khraishi, E. D. Auyang, *Surg. Endosc.* **2016**, *30*, 3250.
17. P. J. Cundy, G. Antoniou, A. Mascarhenas, B. J. C. Freeman, W. J. Cundy, *Spine (Phila Pa 1976)* **2020**, *45*, 1619.
18. N. J. Hallab, *SAS J.* **2009**, *3*, 143.
19. S. L. Wright, F. J. Kelly, *Environ. Sci. Technol*. **2017**, *51*, 6634.
20. UK Parliament. Microplastic pollution. Commons Select Committees, *26*, **2016**.
21. M. Smith, D. Love, C. Rochman, R. Neff, *Curr. Environ. Health Rep.* **2018**, *5*, 375.
22. GESAMP Report: Sources, fate and effects of microplastics in the marine environment: part two of a global assessment. IMO/FAO/UNESCO-IOC/UNIDO/WMO/IAEA/UN/UNEP/ UNDP Joint Group of Experts on the Scientific Aspects of Marine Environmental Protection 2016:220 p.
23. D. M. Brown, M. R. Wilson, W. MacNee, V. Stone, K. Donaldson, *Toxicol. Appl. Pharmacol.* **2001**, *175*, 191.

24. R. S. Labow, E. Meek, J. P. Santerre, *Biomaterials* **2001**, *22*, 3025-33.
25. M. J. Wiggins, B. Wilkoff, J. M. Anderson, A. Hiltner, *J. Biomed. Mater. Res.* **2001**, *58*, 302.
26. M. T. Wolf, C. L. Dearth, LoPresti ST Ranallo, L. E. Carey, K. A. Daly, B. N. Brown, S. F. Badylak. *Biomaterials* **2014**, *35*, 6838.
27. A. L. Nolfi, B. N. Brown, R. Liang, S. L. Palcsey, M. J. Bonidie, S. D. Abramowitch, P. A. Moalli, *Am. J. Obstet. Gynecol.*, **2016**, *215*, 206.
28. M. Geiser, S. Schurch, P. Gehr, *J. Appl. Physiol.* **1985**, *94*, 1793.
29. C. Vasile, M. Dekker, Handbook of Polyolefins, 2nd ed., rev. and expanded, CRC Press, New York **2000**.
30. J. Diani. J. Liu, K. Gall, *Society* **2006**, *46*, 1.
31. P. Y. Wong, A. Takeno. S. Takahashi, S. Phang, A. Baharum, *Polymers* **2021**, *13*, 3425.
32. A. D Vethaak, H. A Leslie, *Environ. Sci. Technol.* **2016**, *5*, 6825.
33. T. S. Galloway, *Micro- and Nano-plastics and Human Health*, Springer, New York, **2015**, 343. https://doi.org/10.1007/978-3-319-16510-3_13
34. A. Salvati, C. Aberg, T. dos Santos, J. Varela, P. Pinto, I. Lynch, K. A Dawson, *Nanomedicine: NBM* **2011**, *7*, 818.
35. J. J Rennick, A. P. R Johnston, R. G Parton, *Nat. Nanotechnol.* **2021**, *16*, 266.
36. G. Rossi, J. Barnoud, L. Monticelli, *J. Phys. Chem. Lett.* **2014**, *2*, 241.
37. A. Anderson, A. Andrady, C. Arthur, J. Baker, H. Bouwman, S. Gall, V. Hildalgo-Ruz, A. Köhler, K. Lavender Law, H. A. Leslie, P. Kershaw, S. Pahl, J. Potemra, P. Ryan, Shim W Joon, R. Thompson, H. Takada, A. Turra, A. D Vethaak, K. Wyles, (GESAMP Reports&Studies Series; No. 90). International Maritime Organization, **2016**
38. T. S Galloway, *Marine Anthropogenic Litter*, Springer **2015**, 343.
39. A. D. Talley, B. R. Rogers, V. Iakovlev, R. F. Dunn, S. A. Guelcher, *J. Biomater. Sci. Polym. Ed.* **2017**, 1.
40. N. T. H. Farr, B. Klosterhalfen & G. K. Noé, *J. Biomed. Mater. Res. B Appl.* **2023**, *111*, 5, 1142.
41. J. Fang, L. Zhang, D. Sutton, X. Wang, T. Lin, *J. Nanomater.* **2012**, *2012*. Article ID 382639.
42. J. N. Barbosa, P. Madureira, A. M. Barbosa, P. A. Aguas, *J. Biomed. Mater. Res. A* **2006**, *76*, 737.
43. P. Thomsen, C. Gretzer, *Curr. Opin. Solid State Mater Sci.* **2001**, *5*, 163.
44. B. G. Keselowsky, D. M. Collard, A. J. Garcia, *Biomaterials* **2004**, *25*, 5947.
45. N. Farr, J. Thanarak, J. Schäfer, A. Quade, F. Claeyssens, N. Green & C. Rodenburg, *Adv. Sci.* **2021**, *8*.
46. S. Kamath, D. Bhattacharyya, C. Padukudru, R. B Timmons, L. J Tang, *Biomed. Mater. Res. A* **2008**, *86*, 617.
47. A. S. Nielsen, D. N. Batchelder, R. Pyrz, *Polymer* **2002**, *43*, 2671.
48. T. Furukawa, H. Sato, Y. Kita, et al. *Polym. J.* **2006**, *38*, 1127.
49. T. Sundell, H. Fagerholm, H. Crozier, **1996**, *37*, 3227.

SUPPORTING INFORMATION

Additional supporting information can be found online in the Supporting Information section at the end of this article.

How to cite this article: N. T. H. Farr, C. Rauert, A. J. Knight, A. I. Tartakovskii, K. V. Thomas, *Nano Select*. **2023**, *4,* 395.
https://doi.org/10.1002/nano.202200243